Channel Blocking Properties of a Series of Nicotinic Cholinergic Agonists

Alison A. Carter and Robert E. Oswald
Department of Pharmacology, College of Veterinary Medicine, Cornell University, Ithaca, New York 14853 USA

ABSTRACT Inhibition of the nicotinic acetylcholine receptor (nAChR) by channel blockade has been demonstrated with a variety of large organic cations, including several nicotinic agonists. We have studied the kinetics of channel blocking of a series of agonists which vary systematically in size and hydrophobicity due to a hydrocarbon chain from one to six carbons in length, as well as one agonist with a tertiary isomer of one hydrocarbon chain. Single-channel recording was used in combination with three different analysis techniques for determining the kinetic and equilibrium parameters of channel blockade. With an increasing number of methylenes, the blocking rates were essentially constant and the unblocking rates decreased exponentially. This is consistent with studies of the blocking properties of alcohols at the nAChR channel (1). Also, a linear decrease in the depth to which the larger agonists penetrate the membrane spanning region of the channel was observed. The three smaller agonists, however, all traverse approximately 75% of the membrane field, in agreement with previous measurements of the location of the narrowest region of the channel, the selectivity filter.

INTRODUCTION

Nicotinic acetylcholine receptors (nAChR) are ligand-gated receptor-channel proteins found in the vertebrate neuromuscular junction, nerve cell membranes, and the electroplaque of the electric fish. The skeletal muscle and the electroplaque receptor is composed of four different subunits ($\alpha_2\beta\gamma\delta$) arranged in a rosette forming an integral membrane ion channel (2). Structural studies indicate that the channel has a large vestibule which protrudes about 7 nm from the extracellular surface, with a diameter of about 2.5–3 nm at the mouth (2). Studies of both structure and function suggest the vestibule is negatively charged, enhancing the attraction of permeant cations (3, 4). The vestibule is believed to lead to a narrow transmembrane region of the channel, which contains the filter for selection of permeant ions (5). The narrow region opens to a smaller vestibule on the intracellular side.

The optimal geometric requirements for an agonist of the nAChR are a cationic head (e.g., a quaternary ammonium group) and a hydrogen bond acceptor (e.g., a carbonyl oxygen) separated by 5.9 Å (6). However, more subtle structural alterations to an agonist can affect its function at the receptor-channel (7). By using the technique of single-channel recording, we have studied the effects of varying the structure of a synthetic agonist, 1,1-dimethyl-4-acetylpiperazinium iodide (PIP (8)), which is held by its ring structure in approximately the correct configuration for binding (the quaternary amine is 6.1 Å from the van der Waals extension of the carbonyl oxygen). Therefore, it is not only a very potent agonist, but due to the lack of an ester function, it is also stable to acetylcholinesterase. Its stability allows for a wide range of structural modifications in order to probe the nAChR channel structure-function relationship.

Many agonists with structures related to PIP have been tested at both the nicotinic and muscarinic receptors using radioligand binding (9). PIP was found to be far more selective for the nicotinic receptor. In this paper, we have studied the properties of a series of six PIP derivatives with a carbon-chain tail of increasing length, and one PIP derivative with a branched isomer of the alkyl group. The agonists vary mainly is size and hydrophobicity, for which we use the hydrophobic surface area as a measure. While some interesting comparisons can be made among the agonists in binding to and activation of the receptor channel, this paper will be concerned primarily with the most striking difference in function: the channel blocking properties of the series of agonists.

Self-inhibition of nicotinic agonists by channel blocking has been demonstrated with a variety of agonists: acetylcholine (ACh) (10); ACh, suberyldicholine and carbamylcholine (11, 12); suxamethonium (13). These studies have provided important information on the interaction of compounds with the lining of the narrow region of the channel. Here, we present the results of a systematic series of blockers with which we have further probed this region of the channel's structure.

Received for publication 19 January 1993 and in final form 5 May 1993.

Address reprint requests to Robert E. Oswald at the Department of Pharmacology, College of Veterinary Medicine, Cornell University, Ithaca, NY 14853. Tel.: 607-253-3877; Fax: 607-253-3659; E-mail: oswald@pharma.vet.cornell.edu.

Abbreviations used: ACh, acetylcholine; DMEM, Dulbecco's modified Eagle medium; FBS, fetal bovine serum; HEPES, *N*-(2-hydroxyethyl)-piperazine-*N'*-2-ethanesulfonic acid; nAChR, nicotinic acetylcholine receptor; PIP, 1,1-dimethyl-4-acetylpiperazinium iodide; pdf, probability density function; QA, quaternary ammonium; Sub, suberyldicholine.

0006-3495/93/08/840/12 $2.00

MATERIALS AND METHODS

Maintenance of cell line

The clonal mouse cell line BC_3H-1 (American Type Culture Collection, Rockville, MD), which expresses the skeletal muscle nAChR (14), was grown in Dulbecco's modified Eagle's medium with 10% fetal bovine serum (FBS) plus 3 ml of penicillin-streptomycin/500-ml bottle of medium and kept at 37°C in 10% CO_2. Cells were passaged at 80% confluency

(every 4–6 days) and plated in Corning 35-mm dishes at 8 $\times 10^3$ cells/ml (day 0). 24 h later (day 1), the medium in the dishes was replaced with low-serum medium (0.5% FBS) to induce differentiation (15). On day 5, the plated cells were fed with fresh low-serum medium and used for recording on days 7–11. The cells were not used past 30 passages.

Organic synthesis

The synthesis of the parent compound, 1,1-dimethyl-4-acetylpiperazinium iodide (PIP), is described by Spivak et al. (8). The derivatives of PIP were synthesized in the same manner with the appropriate anhydride substituted (equal number of moles) for acetic anhydride: propionic anhydride for ethylPIP, butyric anhydride for propylPIP, valeric anhydride for butylPIP, hexanoic anhydride for pentylPIP, heptanoic anhydride for hexylPIP, and trimethylacetic anhydride for *tert*-butylPIP. The syntheses were verified by ^{1}H NMR spectroscopy at 400 MHz (Varian XL400 spectrometer, Sunnyvale, CA).

Electrophysiology

Single channel currents were recorded in the cell-attached or inside-out configuration (16). A Ringer's solution of 147 mM NaCl, 5.4 mM KCl, 1.0 mM $MgCl_2$, and 10 mM HEPES was used in the bath and in the pipet. Pipets were pulled from borosilicate glass (10–20 MΩ) and coated with Sylgard to within 20 mm of the tips. The temperature of the bath was held at 15 ± 0.3°C (Medical Systems, Inc., Greenvale, NY, bipolar temperature controller model TC-202). The Dagan patch clamp amplifier was used to acquire the data, which were then filtered (Frequency Devices, Haverhill, MA, 8-pole Bessel filter) before being stored on videotape (Sony LS750 ES). Resting potentials of all cells tested were 27–30 mV.

Analysis techniques

In order to compare the kinetic properties of the synthetic agonists, we have used two models: one which is sufficient for our purposes at low agonist concentration where the channel may open from the singly liganded or the doubly liganded state of the receptor (7, 17, 18):
Model 1

$$\begin{array}{ccc} R & \rightleftharpoons & AR & \rightleftharpoons & A_2R \\ & & \downarrow\uparrow & & \downarrow\uparrow\alpha \\ & & AR^* & & A_2R^* \end{array} \qquad (1)$$

A = agonist
R = receptor
$*$ = open channel, passing current

And a second model for high agonist (blocker) concentrations in which the majority of open events are due to the doubly liganded state of the receptor (7, 17, 18; Carter, unpublished observations). An additional closed state is included where the open channel is sequentially blocked by a third agonist (blocker) molecule (19, 20):
Model 2

$$R \rightleftharpoons AR \rightleftharpoons A_2R \underset{\alpha}{\rightleftharpoons} A_2R^* \overset{k_{+b}}{\underset{k_{-b}}{\rightleftharpoons}} A_2RA \qquad (2)$$

A = agonist
R = receptor
$*$ = open channel, passing current

Quantitation of our observations required three separate techniques, two for the smaller drugs (faster blockers) and one for the larger drugs (slower blockers). All three techniques make use of Eyring rate theory and assume a single binding site in the narrow region of the channel. This assumption is justified by several observations. From the concentration independence of the permeability ratio of lithium to ammonium, Dani (21) suggests that one binding site is present in the permeation pathway of the narrow region. This is further substantiated by his measurement of the length of the narrowest region by streaming potentials (0.3–0.6 nm) which indicates that more than one binding site in this short distance would be unlikely. Furthermore, with the overwhelming evidence that the uncharged M2 helices line the pore (22–25), the possibility of multiple binding sites for cations (i.e., at negatively charged residues) in the narrow region becomes even more unlikely. Therefore, the two-barrier one-site Eyring rate theory model is not an unreasonable approximation.

Woodhull analysis

Woodhull (26) developed a method for measuring equilibrium constants for very fast blockers by taking advantage of the decrease in current observed in whole-cell recordings. This has been extended to single-channel records for which rapid blocking rates result in a decrease in current due to the limited bandwidth of the recording devices (11). Since the kinetics of blocking are voltage-dependent (for a charged blocker), the apparent decrease in current is a function of voltage. Therefore, *i–V* curves at blocking concentrations are used for fitting with Model 3, below.

The model consists of a forward rate (k_{+b}) of blocking from the extracellular side where the blocker concentration is high, a backward rate (k_{-b}) of unblocking to the extracellular side, and a forward rate (k_p) of unblocking to the intracellular side. k_p is nonzero only if the blocker is small enough to squeeze through the selectivity filter, and the membrane is hyperpolarized enough to provide sufficient driving force. Even in these cases, k_p is assumed to be small enough so that no significant amount of blocker accumulates intracellularly; therefore, a constant describing the rate of blocking from the intracellular side is unnecessary. Equations for the rate constants are obtained from the two-barrier, one-site Eyring rate theory and are given in more detail in the appendix of Woodhull (26). The variables G_0, G_1, H_0, H_1 and the single channel conductance, g, are used as the floating parameters when fitting the model to data. These ratios are

defined below, where R is the universal gas constant, T is the absolute temperature, F is Faraday's constant, z is the valence of the agonist, and δ, called the apparent electrical distance, is the fraction of the total electrical potential drop across the membrane, per unit charge on the blocking ion, from the extracellular surface to the blocking site. Since the membrane is thin, the potential drop is approximately linear and δ may correspond to the fraction of the membrane penetrated by the ion.

The equation used for fitting the model to data is given by $i'(V)$, which is the current amplitude in the presence of a channel blocker. The current amplitude in the absence of blocker, $i(V)$, is equal to the product of the single channel conductance and the holding potential, V. This unblocked amplitude is multiplied by the probability that the channel is unblocked, thereby allowing ions to permeate it. The value, X_o, is equal to the bulk concentration of the blocker on the extracellular side.

Model 3

$$X_0 \underset{k_{-b}}{\overset{k_{+b}}{\rightleftharpoons}} X - \text{site} \overset{k_p}{\rightarrow} X_1$$

$$i'(V) = \frac{i(V)[1 + G(V)]}{1 + G(V) + X_0 H(V)}$$

$$i(V) = gV \tag{3}$$

$$G(V) = k_p/k_{-b} = G_0 \exp(-G_1 V) \qquad G_1 = zF/2RT$$

$$H(V) = k_{+b}/k_{-b} = H_0 \exp(-H_1 V) \qquad H_1 = z\delta F/RT$$

Recordings were made in the inside-out configuration at holding potentials between −30 and −190 mV. The data were filtered at 0.5–1.5 kHz, digitized at 44 kHz and transferred to a VaxStation II computer. Sections of the data for each holding potential were binned on a point basis into amplitude histograms and fit with Gaussian curves using Marquardt optimization (27) to find the mean current amplitude as a function of voltage. The resulting i–V curves were fit with the Woodhull model for single channel blocking, Model 3 (11), in order to determine several parameters associated with channel block. Our program uses a Simplex optimization routine (28) to achieve the best fit of the model to the data.

FitzHugh-Yellen analysis

Another technique which also relies on a decrease in current from fast blocking events is the FitzHugh-Yellen method (29, 30). This method makes use of not only the decreased amplitude but also the increase in open-channel noise resulting from the unresolved events by using the entire current amplitude distribution, instead of just the mean. The method was derived by FitzHugh (29) who made the analogy between a random, asymmetric (binary) telegraph signal and the binary nature of an ion channel's open and closed states. It was further developed and applied to blocking of an ion channel (a true two-state process) by Yellen (30), where it is assumed that the rate of leaving the open-blocked set of states, α, is much smaller than the blocking rate, k_{+b} (Model 2).

Briefly, the method assumes transitions between two states: 0 and 1 (blocked channel = zero current and open channel = unit current). A first-order filter, with a time constant adjusted to empirically mimic the attenuation of an 8-pole Bessel filter, is applied to the time course of the transitions and allows an analytical solution to be found for the amplitude distribution of the filter output. Providing that the transition rates (k_{+b} and k_{-b}) and/or the filter time constant are sufficiently large, the resulting amplitude pdf of a burst will consist of one peak at a time-averaged amplitude determined by the blocking and unblocking rates (31). The analytical solution of the filtered transitions alone is a β distribution. In order to apply the broadening effect of the unrelated high-frequency noise in experimental records to the distribution, it is convolved with a Gaussian distribution with a mean of zero and a standard deviation equal to that of the baseline noise distribution. The input to the simulation includes: the Bessel filter cut-off frequency, the standard deviation of the baseline noise, the initial guesses at the transition rates, and the amplitude histogram of a single burst, preprocessed as described below. The values of k_{+b} and k_{-b} are then optimized to reproduce the experimental results with a Simplex routine (28) using the least-squares criterion to determine convergence.

Recordings were made at high agonist concentration in the inside-out configuration at a holding potential of −120 mV. The data were filtered at 0.5–1.5 kHz, digitized at 44 kHz and transferred to a VaxStation II computer. Sections of data, consisting of an individual burst with an adjacent section of baseline, were chosen from each record and binned on a point basis into amplitude histograms. This created two peaks for each section of data: one at mean zero representing the baseline noise and one representing the amplitude of the open channel and its associated noise. The two peaks were separated into individual histograms, and the baseline peak was fit with a Gaussian curve to obtain the standard deviation of the baseline noise. The values of the current amplitude in the burst histogram were normalized by dividing by the average unblocked current amplitude. This amplitude is the product of the average unblocked conductance (found from an i–V curve at low agonist concentration) and the membrane potential, −120 mV. Also, the area of the burst histogram was normalized to one, to give a probability distribution of current amplitude. The resulting histogram, with an area of one and a mean between 0 and 1, was fit with the FitzHugh-Yellen simulation of channel blocking as described above.

Time-resolved analysis

If the majority of blocking events are resolvable (k_{-b} is slow enough), then direct measurement of open and closed times within bursts is possible. The average dwell time in a state is equal to the reciprocal of the sum of the transition rate constants leading away from that state. Therefore, using Model 2, the average open-time, τ_o, is equal to $1/(\alpha + k_{+b}[x])$

where [x] is the agonist concentration (19). Measurement of $1/\tau_o$ as a function of concentration leads to a calculation of k_{+b} from the slope. The average blocked time, τ_b, would be equal to $1/k_{-b}$.

Recordings were made in the cell-attached configuration. The holding potential in all cases was −90 mV, with a reversal potential of +30 mV, giving a total membrane potential of −120 mV. The data were filtered at 5 kHz and digitized at 44 kHz before being transferred to the VaxStation II. Events were detected with a semi-automated threshold-crossing program developed in the lab, which allows viewing of all events and the option to interrupt for correction. The smallest resolvable event was measured at 0.05 ms. Open- and closed-time analyses were performed on a Sun 4/330 computer (Sun, Mountain View, CA) with a maximum likelihood procedure which allows fitting with up to four exponential components. The closed-times were corrected for missed brief closures (32). The smallest time constant of the distribution, which remained relatively constant over concentration, was taken to be the average blocked time. The open-times were corrected for both missed brief openings and missed brief closures by using the resolvable fraction of events in the pdf of the shortest closed-time as the correction factor.

Molecular structure calculations

The agonist structures were calculated by McGroddy (33) using the AM2 semi-empirical molecular orbital method within MOPAC. The values for the van der Waals volumes and the hydrophobic surface areas were calculated on a Silicon Graphics Iris 4D/220 computer using the molecular modeling program, Quanta (Molecular Simulations, Inc.).

RESULTS

Model for sequential channel blockade

The data must fulfill several criteria to follow the theoretical model of sequential, open-channel blockade (Model 2). With an increase in blocker concentration (in this case agonist concentration), the mean lifetime of the open state decreases due to blocking interruptions and the average duration of

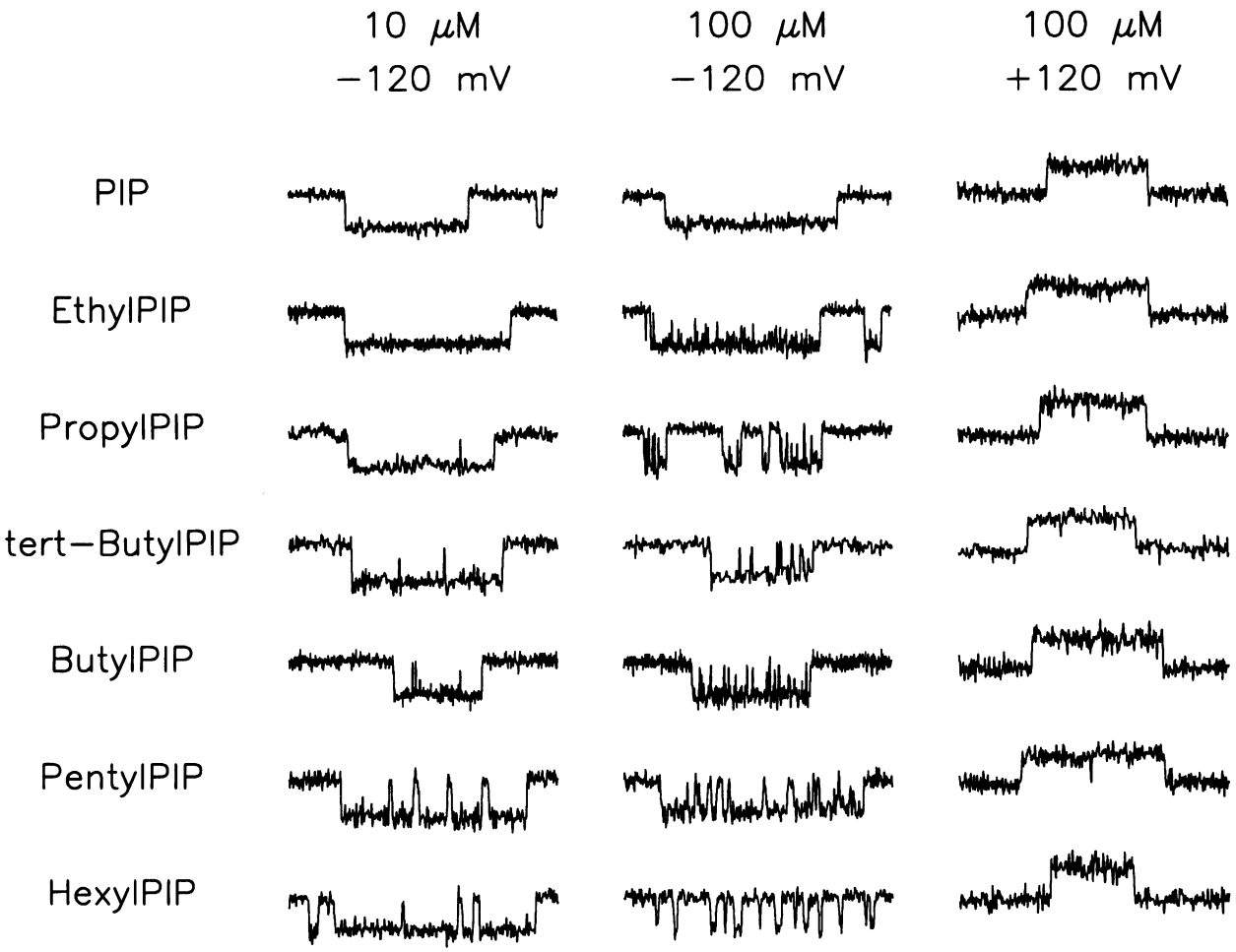

FIGURE 1 Examples of raw data for each of the PIP derivatives collected at different concentrations and membrane potentials. For data at −120 mV, downward deflections represent channel openings. For data at +120 mV, upward deflections represent channel openings. Recordings were made in either the cell-attached or inside-out configurations.

bursts of open-blocked events increases, while the total length of open-time per burst remains constant (19, 32). Also, at high concentrations of blocker, a new component appears in the probability density function (pdf) of the closed-times for which there is an increase in the corresponding area with increasing concentration (19). Another indication of channel blockade, in the case of a charged blocker, is a voltage dependence of the block.

Some of these criteria are illustrated qualitatively in Fig. 1. An increase in the concentration of agonist from 10 to 100 μM applied externally, with the membrane hyperpolarized to −120 mV, resulted in a shortening of the open events. We found no evidence of channel blocking for any of the compounds under depolarizing conditions of +120 mV. Additionally, some differences among the agonists in their blocking properties are evident in the raw data; for instance, with increasing numbers of methylenes in the carbon chain tail, the lengths of the blocked-times appear longer, moving the agonists from the range of "fast" to "intermediate" blockers (5). Also, although a systematic difference in the frequency of blocking among the agonists seems to be present, this turns out to be an artifact of time resolution for the fast blockers, as will be described below.

More quantitative proof of channel blockade is shown in Fig. 2. For six of the agonists, the average open-time, burst duration, and total open-time per burst are plotted versus concentration. The burst durations were found by choosing a closed-time threshold where the number of openings per burst appeared to plateau. These thresholds varied from 0.15 ms for PIP up to 3.2 ms for hexylPIP. For the larger, intermediate drugs, a pronounced decrease in mean open-time is accompanied by an increase in burst duration, while the total open-time per burst remains fairly constant. The decrease in mean open-time for the smaller, fast drugs is less obvious, as is the increase in burst duration. The total open-time per burst increases along with the burst duration, presumably due to the short length and lack of resolution of most of the blocking events.

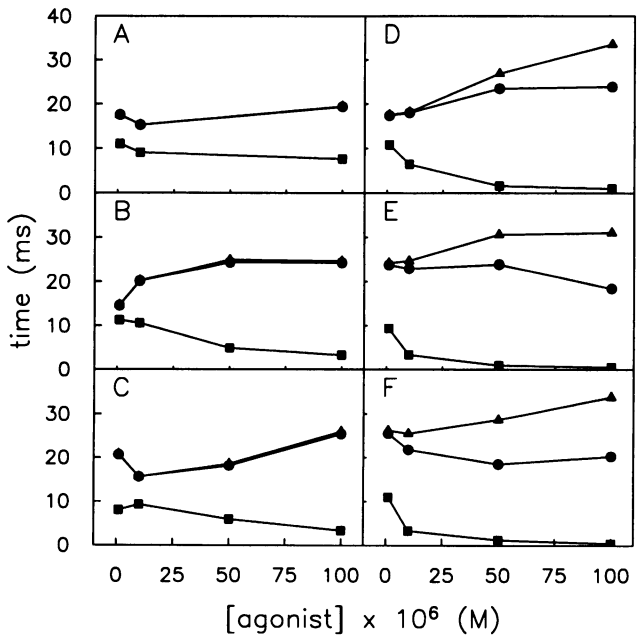

FIGURE 2 Sequential channel block criteria for average open-times (■), burst durations (▲), and total open-time per burst (●) for (*A*) PIP, (*B*) ethylPIP, (*C*) propylPIP, (*D*) butylPIP, (*E*) pentylPIP, and (*F*) hexylPIP.

The data appear to follow the criteria for sequential channel block; however, complicating factors are present. First, the average length of time spent in the A_2R state (Model 2) has been shown to be quite short (about 0.05 ms (7)). With the above burst thresholds, any dwells in this state which are flanked by openings would be mistaken for blocking events. Our observation is that very little blocking occurs at concentrations of 1 μM or less (i.e., recordings at 100 nM yield mean open-times similar to those at 1 μM). At 1 μM, the mean burst duration is only slightly greater than the mean total open-time per burst, both of which are in turn approximately twice the mean open-time for all six agonists. This may be indicative of an average of one dwell in the A_2R state per burst. Second, since the blocking agents are also agonists, an increase in blocker concentration results in a higher frequency of channel activation and a shorter time between successive openings of different channels. For concentrations of 100 μM and above, this occasionally resulted in a poorly defined burst threshold (no plateau, although often a change in slope was present). In these cases, a threshold from a lower concentration of the same drug was used.

Since these complications affect only the burst duration and total open-time per burst, they do not affect our results which rely on average open-time, average blocked-time, or a decrease in conductance from a large amount of fast blocking. The average blocked-time may have been slightly contaminated by the A_2R state; however, at the concentrations studied, the number of blocking events was much greater than the number of dwells in the A_2R state within bursts.

Woodhull analysis

For the faster blockers (PIP, ethylPIP, propylPIP, and *tert*-butylPIP), at sufficiently high concentrations, an apparent decrease in the single channel conductance was observed, because the rapid closures exceeded the bandwidth of the recording devices. Therefore, we were able to use the Woodhull Model (Model 3, in Materials and Methods) adapted for single channel currents (11) to calculate: (*a*) the equilibrium dissociation constants (K_B) at the binding site within the open channel, (*b*) the fraction of the total potential drop across the membrane, δ, measured from the extracellular surface of the membrane to the blocking site, and (*c*) the probability of the agonist being pulled entirely through the channel during extreme hyperpolarization.

Single channel currents were recorded in the inside-out configuration for each agonist at three different concentrations: one low concentration in order to achieve a good estimate for the unblocked conductance, *g*, and two higher concentrations at which significant blocking occurred. Recordings were made over a range of hyperpolarized poten-

tials. The resulting *i–V* curves were fit with Model 3 (Fig. 3) to determine the values of the parameters, which are listed in Table 1.

As the value of G_0 ($= k_p/k_{-b}$) decreases, the tendency of the agonist to permeate the channel as opposed to unblocking to the extracellular surface decreases. This ratio is small for all four agonists and decreases as the agonist alkyl group increases in size, undergoing a precipitous drop at *tert*-butylPIP. This suggests that the larger agonists are less likely to permeate the channel. The value of H_0 gives the ratio of k_{+b}/k_{-b} at 0 mV. As the alkyl group increases in size, the ratio increases, indicating an increase in affinity for the blocking site(s). From the value of H_1 we find δ, which can also be an approximate indication of the depth to which the blocker penetrates the channel. In this case, the three smallest agonists block at the same site, about 3/4 of the way through the membrane-spanning region of the channel, while the larger *tert*-butylPIP does not penetrate this far.

The calculated value of G_1 gives a value of approximately +2 for the valence, z, of the three normal alkyl derivatives and +0.1 for *tert*-butylPIP. Fixing G_1 to 0.02 mV^{-1}, corresponding to a valence of +1 (which might be expected for these compounds), did not provide an adequate fit to the data. Valence calculations greater than +1 have been noted previously (11). A valence of +2 could arise from the presence of two cations (two agonists or one agonist plus a trapped inorganic ion) within the channel or possibly from the polarization of the amide nitrogen per carbonyl oxygen by amino acids lining the channel. The charge on *tert*-butylPIP may be related to the modified charge distribution observed for this derivative in semi-empirical molecular orbital calculations (33). These calculations suggest that all derivatives except *tert*-butylPIP exhibit a significant partially negative charge on the carbon bonded to the carbonyl carbon (e.g., the methyl carbon on PIP). In *tert*-butylPIP, the partial negative charge is much smaller, but it is distributed among three methyl groups. In addition, a change in pore structure could account for these valence calculations.

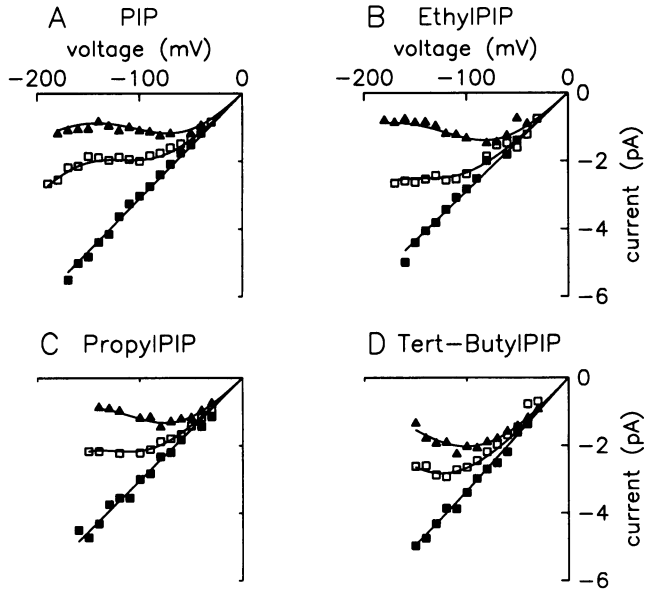

FIGURE 3 Single-channel *i–V* curves with Woodhull model fits for (*A*) PIP at 10 mM (▲), 3 mM (□), and 1 μM (■); (*B*) ethylPIP at 4 mM (▲), 800 μM (□), and 1 μM (■); (*C*) propylPIP at 3 mM (▲), 800 μM (□) and 1 μM (■); (*D*) *tert*-ButylPIP at 1 mM (▲), 400 μM (□), and 10 μM (■). For each agonist, fits were done simultaneously to all three concentrations.

FitzHugh-Yellen analysis

By using Woodhull analysis, we are able to calculate the equilibrium dissociation constant, K_B (which is equal to the ratio $(k_p + k_{-b})/k_{+b}$) for the smaller, fast blockers at 0 mV. However, variations with structure in the values of the individual rate constants k_{-b} and k_{+b} would be of considerable value for understanding the molecular basis of this effect. Direct calculation of these two rate constants from resolved open- and closed-times is possible for the larger agonists (described below), but not for the smaller ones which act too quickly (k_{-b} too large) to resolve the majority of blocking events. However, the FitzHugh-Yellen method, which is similar to the Woodhull method in that it takes advantage of the reduction in single channel amplitude due to unresolved fast blocking, can be used to calculate k_{+b} and k_{-b}. The details of this technique are described in Materials and Methods.

Examples of the amplitude histograms for each of the four agonists are shown (Fig. 4) at a membrane potential of −120 mV and the concentration indicated, with their corresponding convolved β-distribution fits. The values for k_{+b} and k_{-b} are averages of fits to between 6 and 11 bursts. For these agonists, the k_{+b} values are roughly similar; however, there is a marked decrease in the values of k_{-b} with increasing alkyl group size (Table 2).

The equilibrium dissociation constants, K_B, can be calculated at −120 mV with the ratio k_{-b}/k_{+b}. These can be compared to the dissociation constants ($(k_p + k_{-b})/k_{+b}$) from the Woodhull method (since the Woodhull Model allows for permeation) by taking the expression $(1 + G(-120))/H(-120)$ and substituting −120 mV for V and the calculated values of G_0, G_1, H_0, and H_1 for each agonist. The dissociation constants calculated with both methods are shown in Table 2 and are in very close agreement.

Time-resolved method

For the slower blockers, the majority of the blocking events were resolvable, and so, with correction for inevitable missed events, direct measurements of open- and closed-times were used to calculate the blocking and unblocking rates for each agonist (butylPIP, pentylPIP, hexylPIP). Single channels were recorded for each agonist at three different concentrations, and at three different hyperpolarized potentials. The agonist concentrations ranged from 10 to 100 μM, where the majority of openings (80–90%) are due to the doubly liganded state of the receptor channel and where a significant amount of blocking occurs. As the concentration increases, more blocking events occur, shortening the durations of the

TABLE 1 Title

	PIP	EthylPIP	PropylPIP	*tert*-ButylPIP
G_0	0.0023	0.0016	0.0010	8.6×10^{-8}
G_1 (mV^{-1})	0.043	0.040	0.047	0.002
H_0 (M^{-1})	10.17	15.10	20.94	55.59
H_1 (mV^{-1})	0.031	0.031	0.032	0.025
g (pS)	31.0	29.1	30.2	33.7
δ	0.77	0.77	0.79	0.62

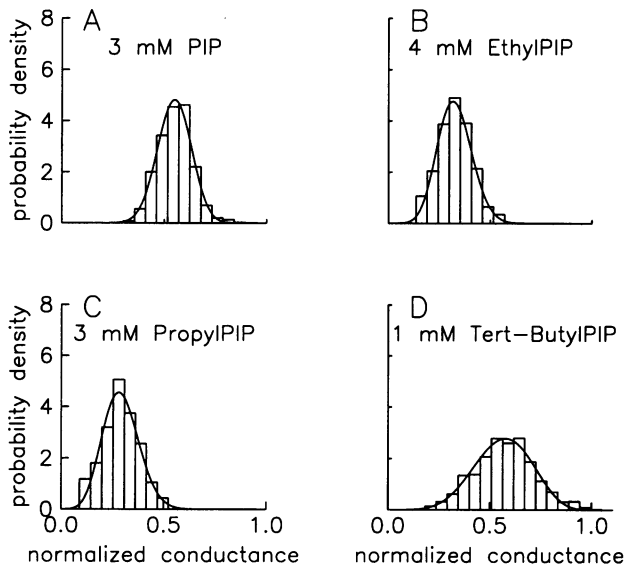

FIGURE 4 Single-channel amplitude histograms with FitzHugh-Yellen fits to (*A*) 3 mM PIP, (*B*) 4 mM ethylPIP, (*C*) 3 mM propylPIP, and (*D*) 1 mM *tert*-butylPIP.

open-times within each burst. For each holding potential, the reciprocal of the doubly liganded mean open-time was plotted as a function of concentration [x], and then fit, by linear least squares, with the equation: $1/\tau_o = \alpha + k_{+b}[x]$ (Fig. 5 *A*), where α is the rate of channel closing as shown in Model 3. Therefore, the slope of each line gives the forward blocking rate, k_{+b}, which is a function of voltage according to the Eyring rate theory equation: $k_{+b} = b \exp(-z\delta FV/2RT)$. The pre-exponential factor, b, is the voltage-independent component of the rate constant containing, for instance, the correction factor for the bulk concentration of blocker within the vestibule of the channel and the voltage-independent part of the activation energy. Plotting the natural log of k_{+b} versus voltage (Fig. 5 *B*) gives a straight line with a slope from which δ can be determined.

At concentrations for which a significant amount of blocking occurs, the receptors are rarely unliganded, and the closed-time histograms were dominated by two to three exponential components corresponding to closed states of the channel, including the blocked state (32). The component in the closed-time histograms which represents the blocked state of the channel, τ_b, remains constant with increasing concentration and accounts for an increasing fraction of the closed-time pdfs (Fig. 6). The reciprocal of τ_b gives the unblocking rate constant, k_{-b}, which decreases with an increasing number of methylenes in the carbon chain tail (Table 2). The ratio of k_{-b}/k_{+b} gives the equilibrium dissociation constant, K_B, for a membrane potential of −120 mV.

Comparison of rate constants

The equilibrium dissociation constant K_B at the blocking site(s) in the nAChR channel decreases with an increase in the number of methylenes in the carbon chain tail of an agonist. This is true for the values of K_B found from the Woodhull method, the FitzHugh-Yellen method and the time-resolved method at −120 mV. Fig. 7 and Table 2 show for all the *n*-alkyl agonists, regardless of the analysis technique used, that this is due to an approximately exponential decrease in the unblocking rate constant, k_{-b}, while the blocking rate constant, k_{+b}, remains fairly constant. The average value of k_{+b}, calculated from only the *n*-alkylPIP derivatives, is $2.65 \times 10^7\ M^{-1}\ s^{-1}$. ButylPIP and *tert*-butylPIP have nearly identical values of k_{+b}. The linear least squares fit to $\ln(k_{-b})$ versus the number of methylenes gives a slope of −1.01. The natural log of K_B [$\ln(k_{-b}/k_{+b})$] versus the number of methylenes will give a linear decrease with the same slope of −1.01. Therefore, the change in free energy between agonist bound and unbound to the blocking site, $\Delta G = RT \ln K_B$, is equal to −2.42 kJ/mol per additional methylene. This change in free energy based on the addition of one methylene suggests a largely hydrophobic interaction of these agonists within the channel. Among the *n*-alkyl derivatives, the volumes and hydrophobic surface areas increase systematically with each additional methylene, as expected (Table 3). ButylPIP and its isomer *tert*-butylPIP have very similar volumes, but the hydrophobic surface area of *tert*-butylPIP falls between those of propylPIP and butylPIP. The trend in k_{-b} follows the trend in the hydrophobic surface area, both for the *n*-alkyl derivatives where k_{-b} decreases with increasing hydrophobic surface area and for *tert*-butylPIP for which k_{-b} as well as the hydrophobic surface area fall between those for propylPIP and butylPIP. The trend in k_{-b} also follows the trend in agonist volume for the *n*-alkyl derivatives but not for *tert*-butylPIP.

Apparent electrical distance, δ

The values of δ for all agonists, obtained using the appropriate technique, are summarized in Table 2 and Fig. 8. In the figure, they are displayed as a function of the van der Waals volume and the hydrophobic surface area of each agonist. The agonists block to an average depth of $\delta = 0.78$ up to a

TABLE 2

	k_{+b} ($M^{-1}s^{-1}$) (−120 mV)	δ	k_{-b} (s^{-1}) (−120 mV)	k_{-b}/k_{+b} (M) (−120 mV) FitzHugh-Yellen method	$(k_p + k_{-b})/k_{+b}$ (M) (−120 mV) Woodhull method
PIP	4.2×10^7	0.77	144×10^3	3.43×10^{-3}	3.34×10^{-3}
EthylPIP	4.0×10^7	0.77	89×10^3	2.23×10^{-3}	1.92×10^{-3}
PropylPIP	2.0×10^7	0.79	26×10^3	1.30×10^{-3}	1.31×10^{-3}
tert-ButylPIP	1.8×10^7	0.62	21×10^3	1.17×10^{-3}	0.90×10^{-3}
ButylPIP	1.759×10^7	0.54	10.2×10^3		
PentylPIP	1.732×10^7	0.44	3.6×10^3		
HexylPIP	2.152×10^7	0.32	0.98×10^3		

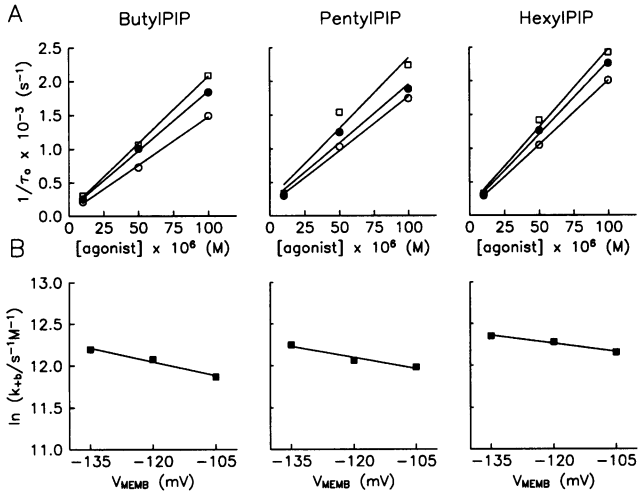

FIGURE 5 Measurement of the blocking rates, k_{+b}, and the apparent electrical distance, δ. (*A*) Reciprocal of doubly liganded open-times versus concentration at membrane potentials of −105 mV (○), −120 mV (●), and −135 mV (□). The fitted lines, found by linear least squares, have slopes equal to k_{+b} and *y* intercepts equal to α. (*B*) The natural log of the values of k_{+b} from the fits in *A* versus membrane potential. The fitted lines, found by linear least squares, have slopes equal to $-z\delta F/2RT$.

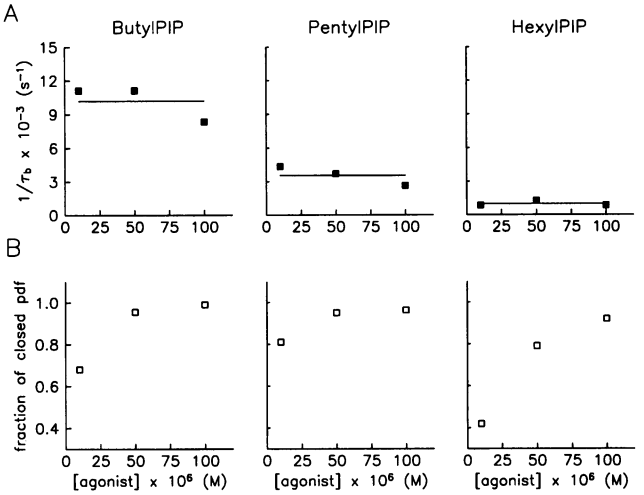

FIGURE 6 Requirements for the time constant in the closed-time distribution which represents the blocked state. (*A*) The time constants remain constant with increasing concentration, and (*B*) the fractions of the closed-time pdf due to this time constant increase with concentration. The reciprocal of the time constant gives the unblocking rate, k_{-b}. For butylPIP, $k_{-b} = 10.2 \times 10^{-3}$ s^{-1}; for pentylPIP, $k_{-b} = 3.6 \times 10^{-3}$ s^{-1}; and for hexylPIP, $k_{-b} = 0.98 \times 10^{-3}$ s^{-1}.

certain size, above which they penetrate to depths which decrease linearly with their size. Of course, the increased size is in the form of a long tail, but if the dipole on each agonist is not large enough to orient the agonist within the channel, then the volume may be thought of roughly as that of a sphere.

As a function of volume (Fig. 8 *A*), the fitted line has a slope of -0.0105 $Å^{-3}$ and a *y* intercept of 2.729. This interpretation may suggest a funnel-shape of the narrow membrane-spanning region of the channel, at least up to about 3/4 of the way through. The slope was based on a fit to only the four largest *n*-alkyl (straight-chain) derivatives. Although the actual value of δ for *tert*-butylPIP is larger than for butylPIP, it falls close to the fitted line and so the two may be within experimental error of each other. This correlation implies that the blocker size may be a determining factor in the depth of penetration.

As a function of hydrophobic surface area (Fig. 8 *B*), the fitted line has a slope of -0.0092 $Å^{-2}$ and a *y* intercept of 2.512. This relation gives a very good fit to all the data, including *tert*-butylPIP. No particular shape of the channel is implied by this relationship, but the hydrophobic character (instead of, or in addition to, the volume) of the drug may affect the points at which they bind within the channel as well.

DISCUSSION

We have used a series of agonists with systematic structural variations to study the structure-function relationship of agonist self-inhibition at blocking site(s) within the ion-channel pore. By increasing the number of methylenes in a carbon-chain tail of the agonist, both its size and hydrophobicity (hydrophobic surface area) are increased. With these increases, the blocking rate, k_{+b}, remains approximately constant, and the unblocking rate, k_{-b}, decreases exponentially. The blocking rate for *tert*-butylPIP is similar to the others, but the unblocking rate is slightly larger than that for butylPIP, in agreement with the order of hydrophobic surface area. We also found that the three smaller agonists penetrate the channel to the same depth, while the four larger ones penetrate to decreasing depths.

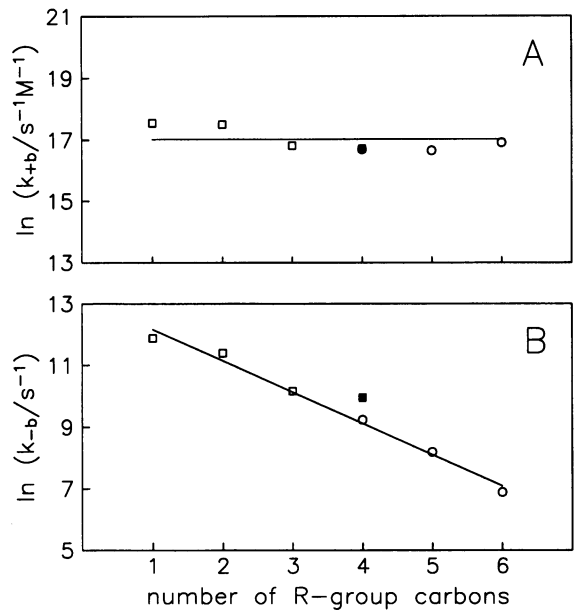

FIGURE 7 Comparison of blocking and unblocking rates for all agonists at a membrane potential of −120 mV. Open squares (□) represent values from the FitzHugh-Yellen method, with a filled square (■) for *tert*-butylPIP, and open circles (*F*) represent values from the time-resolved method. (*A*) The blocking rate, k_{+b}, remains essentially constant. ButylPIP and *tert*-butylPIP values overlap. (*B*) The unblocking rate, k_{-b}, decreases exponentially. *tert*-ButylPIP falls approximately midway between propylPIP and butylPIP.

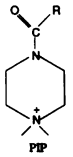

Table 3

	R group	van der Waals Volume (Å^3)	Hydrophobic Surface Area (Å^2)
PIP	CH_3	154.0	155
Ethyl PIP	CH_2CH_3	170.2	176
Propyl PIP	$(CH_2)_2CH_3$	186.7	192
tert-Butyl PIP	$C(CH_3)_3$	207.2	202
Butyl PIP	$(CH_2)_3CH_3$	204.0	210
Pentyl PIP	$(CH_2)_4CH_3$	216.5	225
Hexyl PIP	$(CH_2)_5CH_3$	230.8	240

Rate constants and equilibrium dissociation constants

The exponential decrease in the unblocking rate, k_{-b}, is responsible for a linear decrease in change of free-energy of blocking with increasing numbers of methylenes in the carbon-chain tail. Similar results have been found with *n*-alcohol derivatives acting from both the intracellular side of the channel (cultured rat myotubes (1)) and the extracellular side (BC_3H-1 cells (34)). Murrel et al. (1) found a linear decrease in the change in free energy for blocking with *n*-alcohols ($RT \ln K_B$) for pentanol to octanol, with a slope of −3.30 KJ/mol per additional methylene. This is similar to

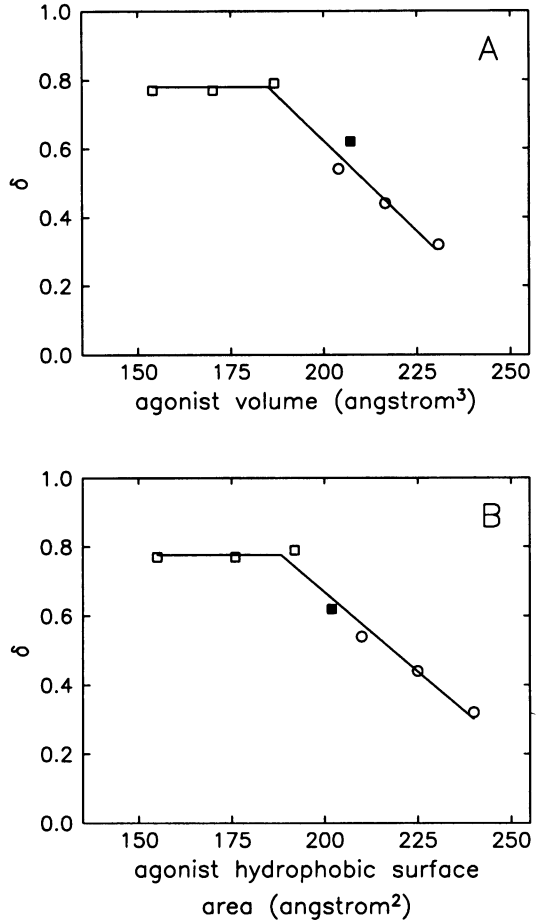

FIGURE 8 Comparison of the apparent electrical distances, δ, for all agonists as a function of (*A*) van der Waals volume and (*B*) hydrophobic surface area. Open squares (□) represent values from the FitzHugh-Yellen method, with a filled square (■) for *tert*-butylPIP, and open circles (○) represent values from the time-resolved method. The linear fit was by linear least squares.

our finding of −2.42 kJ/mol. They also concluded that this large hydrophobic effect was due to a decrease in k_{-b}, while k_{+b} remained fairly constant with no particular trend as the number of methylenes increased. McLarnon et al. (34) also found a linear relationship in $\log_{10}(K_B)$ versus *n*-alcohol from propanol to octanol (which gave a slope for $RT \ln K_B$ versus *n* of −4.55 kJ/mol). These findings support the hypothesis that the membrane-spanning region, M2, which consists of mostly uncharged hydrophobic residues, contributes to the lining of the channel (22, 24, 25, 35–37). In fact, studies have shown that channel block by the local anesthetic, QX222, is reduced not only by mutating the polar residues of the binding site at the 6′ position of M2 to alanines (24), but also by mutating leucine 247 of chick brain α7 to a polar threonine (38). In addition, Leonard et al. (39) were able to enhance QX222 block by mutating the 10′ site to include more hydrophobic residues. These authors suggest that the amino end of the blocker binds to the polar site, while the hydrophobic aromatic end is stabilized by the hydrophobic residues on the externally adjacent turn of the α-helix.

These studies, as well as the correlation of all seven agonists with their calculated hydrophobic surface areas, suggest that the decrease in k_{-b} with increasing alkyl-group size is due to the hydrophobic environment of the channel. However, another possible contribution to an increase in binding affinity has been suggested by Dani (4). The net negative charge of the extracellular vestibule to the channel is shielded to some degree by the cations in solution. Larger ions have a difficult time entering the vestibule, in which case there are fewer of them to shield the negative charge. When a large fraction of the bathing solution is made up of larger ions (as in the case of blocking concentrations of an agonist), less shielding occurs and the net negative charge is stronger, contributing to an increase in the binding affinity of a cationic channel blocker. Therefore, the larger the blocker, the smaller the shielding will be, resulting in higher binding affinities. At several of the concentrations we studied, the agonists do, indeed, account for a small mole fraction of the total cation concentration. These two effects could be separated by testing blockers of various sizes, but lacking the hydrophobic character of those used in this study.

Our results are also consistent with observations of hydrophobic blockers at other channels. Two studies performed on potassium channels of the squid axon yield results similar to ours. Armstrong (40) used a series of alkyl-triethylammonium ions and found a "tighter binding" to the blocking site with longer alkyl chains. French and Shoukimas (41, 42) used both triethyl- and tetraalkylammonium derivatives. They also observed a decrease in the dissociation constant with increasing alkyl chain length. However, in contrast to measurements with our system, Miller (43) noted, at the sarcoplasmic reticulum potassium channel, a strong variation in the blocking rate (k_{+b}) of quaternary ammonium derivatives with increasing numbers of methylenes.

An additional implication of the decrease in k_{-b} with increasing methylenes is the trend seen in the Woodhull parameter G_0 ($= k_p/k_{-b}$). This ratio represents the relative

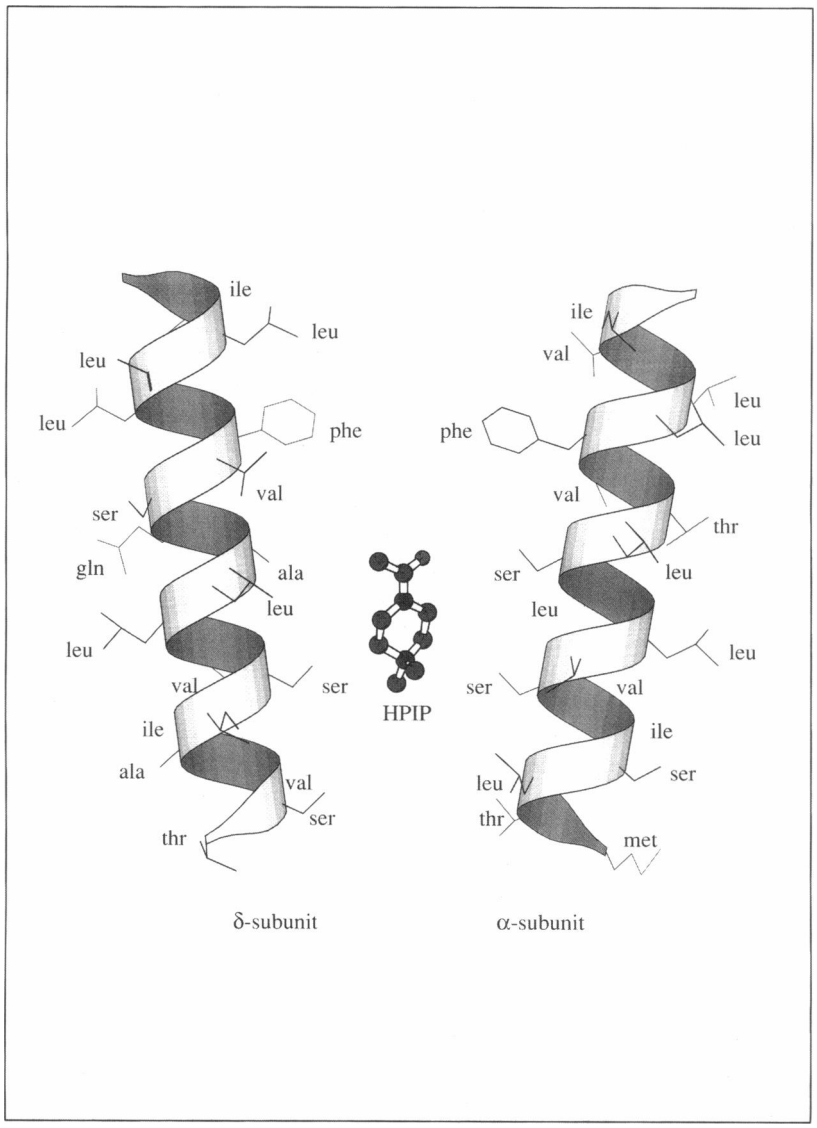

FIGURE 9 Schematic representation of the M2 helices of the α and δ subunit of the BC_3H-1 nAChR drawn as α-helices with PIP drawn to scale with the quaternary amine in approximately the 6′ position. The figure was generated with MolScript (52). The coordinates for the structure were generated with Quanta (Molecular Simulations, Inc.).

likeliness of the blocker to penetrate the channel as opposed to unblocking back to the extracellular side, at 0 mV. The trend in G_0 for the four blockers tested was to decrease with increasing size, suggesting increased difficulty in penetrating with an increase in size. This is especially true for the bulky *tert*-butylPIP, for which there is a precipitous drop in G_0. Given the additional information from the FitzHugh-Yellen method that the denominator, k_{-b}, decreases with increasing size, k_p must decrease even faster, creating an even more pronounced trend of difficulty in penetrating the channel with increased size. Of course, factors other than size may contribute to this trend. There may be a difference among the blockers in their orientation energies or steric abilities to orient within the channel, so that the smaller blockers more easily assume an orientation which allows them to pass through. Or the hydrophobic interactions at the site which contribute to the decrease in k_{-b} may affect k_p as well. However, a study of permeabilities of 52 monovalent cations at the endplate receptor (44) suggest that size is a more important factor of permeability than are specific chemical groups of organic cations.

Structure of the channel

The values of δ for all agonists are given in Table 2. From Woodhull analysis and time-resolved analysis, we found that the agonists block to an average depth of $\delta = 0.78$ up to a certain size, above which they penetrate to depths which decrease linearly with their size. A similar variation in penetration depth has been observed in some potassium channels. Both French and Shoukimas (41, 42) and Swenson (45) concluded that, for channels in the squid axon, the depth of penetration of quaternary ammonium (QA) derivatives was inversely related to the size (the length of an alkyl chain) of the entering ion. Again, the potassium channel in the sarcoplasmic reticulum is different, where Miller (43) found a constant penetration depth for monovalent QAs.

Previous studies of the nAChR have shown that the narrowest part of the channel, the selectivity filter, is located at approximately $\delta = 0.75$–0.8 (11, 46, 47) and has a very short length of 3–6 Å (21). The latter measurement was interpreted to mean that the channel must spread away from this region, into a funnel shape. Additionally, Karlin et al. (48) reported labeling the M1 membrane-spanning region with the intrachannel blocker, quinicrine, despite the overwhelming evidence that M2 lines the channel. Dani (49) suggested that a spreading-out of the M2 helices in the funnel hypothesis might allow the adjacent M1 region to be exposed to the lumen of the channel as well; although, the possibility that the M2 region exists as a β-strand would also allow the M1 region to be exposed to the channel (50).

For the three larger agonists, the difference between the location of the blocking sites is about one-tenth the membrane thickness. Given a membrane thickness of 40 Å, this would mean a difference in location of about 4 Å. The distance between the turns of an α-helix, based on x-ray structures of α-helices in proteins (51), is 5.4 Å, and the distance between the side chains is in the range of 4–7 Å, suggesting that perhaps the larger blockers get "stuck" at the mostly hydrophobic residues on consecutive helix turns (Fig. 9). The excellent linear correlation between δ, and the hydrophobic surface area suggests that the hydrophobic character may also be a determining factor of the depth of penetration.

We thank Leah Goodman for detecting single-channel data, Vijay Kotha for synthesizing and verifying the agonists, Dr. Jerry Wright (National Institute on Alcohol Abuse and Alcoholism) for providing the core of the FitzHugh-Yellen program, and Drs. Linda Nowak and Gregory Weiland (Cornell University) for helpful discussions.

This work was supported by National Institutes of Health grant RO1 NS 18660 and a software grant from Molecular Simulations, Inc. Alison A. Carter was supported by NIH predoctoral training grant T32GM08210.

REFERENCES

1. Murrell, R. D., M. S. Braun, and D. A. Haydon. 1991. Actions of *n*-alcohols on nicotinic acetylcholine receptor channels in cultured rat myotubes. *J. Physiol. (Lond.).* 437:431–448.
2. Brisson, A., and P. N. T. Unwin. 1985. Quaternary structure of the acetylcholine receptor. *Nature. (Lond.).* 315:474–477.
3. Imoto, K., C. Busch, B. Sakmann, M. Mishina, T. Konno, J. Nakai, H. Bujo, Y. Mori, K. Fukuda, and S. Numa. 1988. Rings of negatively charged amino acids determine the acetylcholine receptor channel conductance. *Nature. (Lond.).* 335:645–648.
4. Dani, J. A. 1986. Ion-channel entrances influence permeation: net charge, size, shape, and binding considerations. *Biophys. J.* 49:607–618.
5. Hille, B. 1992. Ionic Channels of Excitable Membranes. Sinauer Associates, Sunderland, MA. pp. 423–444.
6. Beers, W. H., and E. Reich. 1970. Structure and activity of acetylcholine. *Nature. (Lond.).* 228:917–922.
7. Papke, R. L., G. Millhauser, Z. Lieberman, and R. E. Oswald. 1988. Relationships of agonist properties to the single channel kinetics of nicotinic acetylcholine receptors. *Biophys. J.* 53:1–12.
8. Spivak, C. E., T. M. Gund, R. F. Liang, and J. A. Waters. 1986. Structural and electronic requirements for potent agonists at the nicotinic receptor. *Eur. J. Pharmacol.* 120:127–131.
9. Spivak, C. E., J. A. Waters, and R. S. Aronstam. 1989. Binding of semirigid nicotinic agonists to nicotinic and muscarinic receptors. *Mol. Pharmacol.* 36:177–184.
10. Colquhoun, D., and D. C. Ogden. 1988. Activation of ion channels in the frog end-plate by high concentrations of acetylcholine. *J. Physiol. (Lond.).* 395:131–159.
11. Sine, S. M., and J. H. Steinbach. 1984. Agonists block currents through acetylcholine receptor channels. *Biophys. J.* 46:277–284.
12. Ogden, D. C., and D. Colquhoun. 1985. Ion channel block by acetylcholine, carbachol, and suberyldicholine at the frog neuromuscular junction. *Proc. R. Soc. Lond. Ser. B Biol. Sci.* 225:329–355.
13. Marshall, C. G., D. Ogden, and D. Colquhoun. 1991. Activation of ion channels in the frog endplate by several analogues of acetylcholine. *J. Physiol. (Lond.).* 433:73–93.
14. Schubert, D., A. J. Harris, C. E. Devine, and S. Heinemann. 1974. Characterization of a unique muscle cell line. *J. Cell Biol.* 61:398–413.
15. Olsen, E., L. Glaser, J. P. Merlie, R. Sebanne, and J. Lindstrom. 1983. Regulation of surface expression of acetylcholine receptors in response to serum and cell growth in BC_3H-1 muscle cell line. *J. Biol. Chem.* 258:13946–13953.
16. Hamill, O. P., E. Marty, B. Neher, B. Sakmann, and F. J. Sigworth. 1981. Improved patch-clamp techniques for high-resolution current recording from cells and cell-free membrane patches. *Pfluegers Arch. Eur. J. Physiol.* 391:85–100.
17. Labarca, P., M. S. Montal, J. M. Lindstrom, and M. Montal. 1985. The occurrence of long openings in the purified cholinergic receptor channel increase with acetylcholine concentration. *J. Neurosci.* 5:3409–3413.

18. Colquhoun, D., and B. Sakmann. 1985. Fast events in single-channel currents activated by acetylcholine and its analogues at the frog muscle end-plate. *J. Physiol. (Lond.).* 369:501–557.

19. Neher, E., and J. H. Steinbach. 1978. Local anaesthetics transiently block currents through single acetylcholine-receptor channels. *J. Physiol. (Lond.).* 277:153–176.

20. Papke, R. L., and R. E. Oswald. 1989. Mechanisms of noncompetitive inhibition of acetylcholine-induced single-channel currents. *J. Gen. Physiol.* 93:785–811.

21. Dani, J. A. 1989b. Open channel structure and ion binding sites of the nicotinic acetylcholine receptor channel. *J. Neurosci.* 9:884–892.

22. Changeux, J.-P., J. Giraudat, and M. Dennis. 1987. The nicotinic acetylcholine receptor: molecular architecture of a ligand-regulated ion channel. *TIPS.* 8:459–465.

23. Charnet, P., C. Labarca, R. J. Leonard, N. J. Vogelaar, L. Czyzyk, A. Gouin, N. Davidson, and H. A. Lester. 1990. An open-channel blocker interacts with adjacent turns of α-helices in the nicotinic acetylcholine receptor. *Neuron.* 2:87–95.

24. Leonard, R. J., C. G. Labarca, P. Charnet, N. Davidson, and H. A. Lester. 1988. Evidence that the M2 membrane-spanning region lines the ion channel pore of the nicotinic receptor. *Science (Wash. DC).* 242:1578–1581.

25. Giraudat, J., M. Dennis, T. Heidmann, and J.-Y. Chang. 1986. Structure of the high-affinity binding site for noncompetitive blockers of the acetylcholine receptor: serine-262 of the δ subunit is labeled by [^{3}H]-chlorpromazine. *Proc. Natl. Acad. Sci. USA.* 83:2719–2723.

26. Woodhull, A. M. 1973. Ionic blockade of sodium channels in nerve. *J. Gen. Physiol.* 61:687–708.

27. Bevington, P. R. 1969. Data Reduction, and Error Analysis for the Physical Sciences. McGraw-Hill Publishing Co., New York.

28. Caceci, M. S., and W. P. Cacheris. 1984. Fitting curves to data: the simplex algorithm is the answer. *Byte.* 9:340–362.

29. FitzHugh, R. 1983. Statistical properties of the asymmetric random telegraph signal, with applications to single-channel analysis. *Math. Biosci.* 64:75–89.

30. Yellen, G. 1984. Ionic permeation and blockade in Ca^{2+}-activated K^+ channels of bovine chromaffin cells. *J. Gen. Physiol.* 84:157–186.

31. Coronado, R., and C. Miller. 1979. Voltage-dependent caesium blockade of a cation channel from fragmented sarcoplasmic reticulum. *Nature. (Lond.).* 280:807–810.

32. Colquhoun, D., and A. G. Hawkes. 1983. The principles of the stochastic interpretation of ion-channel mechanisms. *In* Single-Channel Recording. B. Sakmann, and E. Neher, editors. Plenum Publishing Corp., New York. 135–174.

33. McGroddy, K. A. 1992. Structures, dynamics, and potencies of cyclic and acyclic nicotinic cholinergic agonists. Ph.D. thesis. Cornell University, Ithaca, NY.

34. McLarnon, J. G., P. Pennefather, and D. M. J. Quastel. 1986. Mechanism of nicotinic channel blockade by anesthetics. *In* Molecular and Cellular Mechanisms of Anesthetics. S. H. Roth, and K. W. Miller, editors. Plenum Publishing Corp., New York. 155–163.

35. Hucho, F., W. Oberthur, and F. Lottspeich. 1986. The ion channel of the nicotinic acetylcholine receptor is formed by the homologous helices M2 of the receptor subunits. *FEBS Lett.* 205:137–142.

36. Imoto, K., C. Methfessel, B. Sakmann, M. Mishina, Y. Mori, T. Konno, K. Fukuda, M. Kurasaki, H. Bujo, Y. Fujita, and S. Numa. 1986. Location of a delta-subunit region determining ion-transport through the acetylcholine-receptor channel. *Nature. (Lond.).* 324:670–674.

37. Dani, J. A., and G. Eisenman. 1987. Monovalent and divalent cation permeation in acetylcholine receptor channels: ion transport related to structure. *J. Gen. Physiol.* 89:959–983.

38. Galzi, J. L., D. Bertrand, A. Devillers-Thiéry, F. Revah, S. Bertrand, and J. P. Changeux. 1991. Functional significance of aromatic amino acids from three peptide loops of the α7 neuronal nicotinic receptor site investigated by site-directed mutagenesis. *FEBS Lett.* 294:198–202.

39. Leonard, R. J., P. Charnet, C. Labarca, N. J. Vogelaar, L. Czyzyk, A. Gouin, N. Davidson, and H. A. Lester. 1992. Reverse pharmacology of the nicotinic acetylcholine receptor. Mapping the local anesthetic binding site. *Ann. NY Acad. Sci.* 625:588–599.

40. Armstrong, C. M. 1971. Interaction of tetraethylammonium ion derivatives with the potassium channels of giant axons. *J. Gen. Physiol.* 58:413–437.

41. French, R. J., and J. J. Shoukimas. 1981. Blockage of squid axon potassium conductance by internal tetra-n-alkylammonium ions of various sizes. *Biophys. J.* 34:271–291.

42. French, R. J., and J. J. Shoukimas. 1985. An ion's view of the potassium channel: the structure of the permeation pathway as sensed by a variety of blocking ions. *J. Gen. Physiol.* 85:669–698.

43. Miller, C. 1982. Bis-quaternary ammonium blockers as structural probes of the sarcoplasmic reticulum K^+ channel. *J. Gen. Physiol.* 79: 869–891.

44. Dwyer, T. M., D. J. Adams, and B. Hille. 1980. The permeability of the endplate channel to organic cations in frog muscle. *J. Gen. Physiol.* 75:469–492.

45. Swenson, R. P. 1981. Inactivation of potassium current in squid axon by a variety of quaternary ammonium ions. *J. Gen. Physiol.* 77:255–271.

46. Adams, P. R. 1977. Voltage jump analysis of procaine action at frog end-plate. *J. Physiol. (Lond.).* 268:291–318.

47. Horn, R., M. S. Brodwick, and W. D. Dickey. 1980. Asymmetry of the acetylcholine channel revealed by quaternary anesthetics. *Science (Wash. DC).* 210:205–207.

48. Karlin, A., P. N. Kao, and M. Dipaola. 1986. Molecular pharmacology of the nicotinic acetylcholine receptor. *TIPS.* 7:304–308.

49. Dani, J. A. 1989a. Site-directed mutagenesis and single channel currents define the ionic channel of the nicotinic acetylcholine receptor. *TINS.* 12:125–128.

50. Akabas, M. H., D. A. Stauffer, M. Xu, and A. Karlin. 1992. Acetylcholine receptor channel structure probed in cysteine-substitution mutants. *Science (Wash. DC).* 258:307–310.

51. Creighton, T. E.. Proteins: Structures and Molecular Properties. 1984. W. H. Freeman and Company, New York.

52. Kraulis, P. J. 1991. MolScript - a program to produce both detailed and schematic plots of protein structures. *J. Appl. Chem.* 24:946–950.